ORIGINAL PAPER

Effect of low vacuum environment on the fused filament fabrication process

Marshall Quinn[1] · Ugo Lafont[2] · Johan Versteegh[3] · Jian Guo[1]

Abstract

The purpose of this research was to investigate the suitability of the Fused Filament Fabrication (FFF) process for low pressure/vacuum environment. This included investigating the ability of an FFF printer to function in a vacuum and evaluation of the dimensional accuracy and mechanical properties of the manufactured components. For this purpose, a commercially available FFF printer using polycarbonate as raw material was placed in a vacuum environment of 10 mbar. Test components were then fabricated in vacuum with a control group fabricated in a normal atmosphere (1 bar). Test components were evaluated for dimensional and mass accuracy, quality and presence of defects. Flexural, tensile and compressive testing was carried out according to ASTM D790, D638 and D695 respectively. Dimensional analysis of components showed equivalent small deviation for both environments. Components fabricated in the vacuum environment had 5.4% higher tensile yield strength and 59% higher extension at break compared to components printed in a normal atmosphere indicating an increased strength and ductility. Components tested in compression had approximately 11.2% higher compressive strength when printed in a vacuum environment. No differences were observed during the flexural test. In space, due to the vacuum environment, polymers and organic material are susceptible to release molecules via an outgassing process. Assessment of the molecular organic contamination generate during the printing process in vacuum is low and seems to mostly originated from the components of the printer. The results provided demonstrated the possibility to use the FFF process in a vacuum environment to fabricate dimensionally accurate, high-quality polycarbonate components with a variety of geometries without loss of mechanical performance. This work provides a proof of concept that FFF can be used to develop out-of-earth manufacturing technologies (in orbit/in space/on planet) allowing part production for new maintenance and repair strategy or to potentially manufacture entire structure more efficiently overpassing launch constrain by using only raw material brought from earth.

Keywords 3D printing · Thermoplastic · FFF · Vacuum · In-space manufacturing

1 Introduction

Having manufacturing capability to produce part out-of-earth/in-space has been identified as a need to enable future mission specially for human spaceflight [1]. There have been several successful demonstrations of the suitability of Fused Filament Fabrication (FFF) technology in zero gravity environment onboard the International Space Station (ISS) [2–6]: 3D printing in zero g demonstrator (3DP), Additive Manufacturing Facility (AMF) from Made In Space, the Italian Space Agency funded "Portable on Orbit Printer 3D" (POP3D) and the REFRABICATOR from Tethers Unlimited. These printers clearly demonstrate the capability of such technology as a reliable manufacturing process in orbit under reduced gravity condition. While these printers have been very successful in laying the groundwork for FFF printing in microgravity, they have several limitations among which the build volume, the potential outgassing/contamination occurring during operation and need for confinement and, their operation within a controlled environment with temperature and pressure identical to the earth environment (1 bar, 25 °C). To enable this technology to manufacture in space/out-of-earth large-scale infrastructure, the process

✉ Ugo Lafont
ugo.lafont@esa.int

1 Aerospace Engineering, Delft University of Technology, Kluyverweg 1, 2629 HS Delft, The Netherlands

2 ESTEC, European Space Agency, Keplerlaan 1, Postbus 299, 2200 AG Noordwijk, The Netherlands

3 Ultimaker B.V., Watermolenweg 2, 4191 PN Geldermalsen, The Netherlands

must be tested and proven to work in a typical space environment characterized, beside a complex radiative environment, by vacuum and extreme temperature range (e.g. − 150 to 150 °C for a conventional range). In this work, we aim to demonstrate the feasibility of using FFF technology in a reduced pressure environment and assess the effect of such environment on the manufactured parts dimension accuracy, mechanical performance and process related molecular contamination aspect. To our knowledge, such data are not available and the result presented are paving the path toward in space manufacturing technology development.

2 Material and methods

2.1 Experimental setup

All manufacturing activities were performed in an ISO8 clean room. The vacuum environment was created using Heraeus VT 6130 M vacuum chamber compatible with pressure down to 10^{-2} mbar connected to a Vacuubrand MD-1 pump. An Ultimaker 2 + FFF printer (Ultimaker B.V) equipped with a 0.4 mm nozzle was used for this experiment. The printer envelope was removed, keeping only the frame. The electronics control board of the printer and power unit were also removed and placed outside the vacuum chamber during the experiment. This was done to eliminate a potential failure of the electronic controller that are not vacuum compatible. Fans that are used for print cooling and nozzle temperature regulation and their associated wiring were removed and not used during the entire experiment. The electronic controller and power unit placed outside the vacuum chamber were re-connected to the printer using dedicated wiring via the specific sealed port available in the vacuum chamber. Removing unnecessary parts was also done aiming to minimize the amount of polymer material that will be exposed to vacuum, limiting material outgassing. Keeping this philosophy in mind, most of the lubricants used by default on moving parts was cleaned off. Removing lubricants will affect the printer functionality in time but this was not considered as a risk for the amount of experiment to be performed. In addition, as the raw material in a shape of filament will be located in the vacuum chamber, only the right amount of filament (~ 2.5 m) was fed into the print head before each printing experiment.

Due to the vacuum environment and related heat transfer problem, the experimental setup has been first optimized [7] involving thermal modeling and monitoring of the temperature of the print head heater, stepper motors, and print bed. This initial phase results in two main optimization. The original extrusion head was replaced by a hot end designed for extrusion of high melting point thermoplastics that allow better decoupling of the thermal load toward the filament

driver. The thermal controller used, optimized to work in the normal environment, was not capable to reach the desired set point leading to strong temperature overshooting when operated in a vacuum. The thermal controller PID (Proportional, Integral, Derivative) values of the print head heater were modified and adjusted to 8.50, 1.55 and 95.00, respectively. This allowed to maintaining reasonable heating time and oscillations around the set temperature limiting overshooting to about 7 °C. The described experimental set up was used to print samples in vacuum (10 mbar) and in normal pressure (1 bar) for comparison. Printing at 1 bar pressure was done with the vacuum chamber close but without applying vacuum thus under normal atmospheric condition (air). This printing condition is identical to any currently applied condition for operating a commercial 3D printer (in air). In this respect, the potential effect of air like contribution to oxidative reaction during material melting/extrusion is not taken into account in this study as considered as normal operating condition for such process. For printing in vacuum, once the vacuum chamber reach 1 mbar (within ~ 35 min of active pumping), the vacuum valve was closed to isolate the chamber and the pump turned off. Printing at 10 mbar was started 10 min after (Fig. 1).

The reference environment was defined as an environment with a pressure of 1 bar, a temperature of 25 °C and 1 g of gravity. The choice of the chamber temperature was also dictated to fit the operating temperature range of the vacuum pump, the vacuum chamber and the printer. The vacuum

Fig. 1 Experimental set up showing the 3D printing inside the vacuum chamber and the electrical connection routing needed to reconnect the printer to the electronic and power board located outside the chamber

environment was chosen to be an environment with a pressure of 10 mbar, a temperature of 25 °C and 1 g of gravity.

2.2 Materials

Black polycarbonate filament (2.85 mm diameter, Ultimaker) with a density of 1.19 g.cm^{-3} was used a raw material source. The choice of material was a tradeoff between the printer capabilities, the mechanical and thermal performance and the wish to use a material with the lowest outgassing properties. This material present a Tg of 112 °C, good mechanical performance and need to be melt-processed at 260 °C. This was a good compromise between commodity thermoplastics easy to print but with low mechanical performance (e.g. Polylactic acid, Acrylonitrile Butadiene Styrene) and high-performance thermoplastics (e.g. Polyetheretherketone) with excellent mechanical performance but that requires high-temperature printing system not possible with the 3D printer used. The produced samples geometry was following the ASTM D638 Type I standard for tensile testing regarding the shape and width of the narrow section (3.2 mm × 13 mm) but with slightly extend length for the end tabs, the ASTM D790 for flexural testing (2 mm × 12.7 mm × 50 mm) and the ASTM D695 standard for compression testing (cylinder of 12.7 mm diameter and height of 25.4 mm). Sample geometry is described in Fig. 2. Five samples per configuration were produced in batch and tested ($n = 5$).

2.3 Printing strategy

Cura 3.0.4. software was used to generate the g-code file used by the printer. The printing parameters and associated
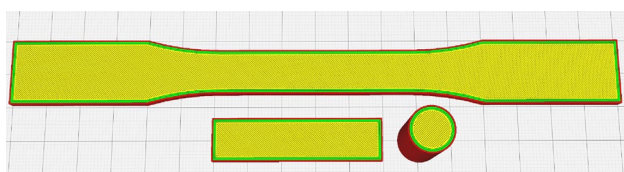
Fig. 2 Scaled test samples type and shape used for tensile testing ASTM D638 Type I (top), flexural testing ASTM D790 (bottom left) and compression testing ASTM D695 (bottom right) showing the infill orientation (−45/45) and the number of perimeters used (3)

printing strategy were fixed as follow: extrusion temperature of 260 °C, build plate temperature of 110 °C, infill printing speed of 45 mm s^{-1}, layer height of 0.2 mm, line width of 0.35 mm, wall thickness of 1.2 mm (3 contours), infill 100% and raster layer orientation of ±45°. Samples were printed by batch of five. The complete Cura printing profile can be found in [7]. The tensile and flexural test sample were printed with their largest surface area in the XY plane. The cylindrical-shaped samples for compression testing were printed in a stand-up position (Fig. 2).

2.4 Characterization techniques

All mechanical tests were performed on a Zwick/Roell 250 kN universal tester. For the compressive testing a preload force of 10 N and a displacement rate of 1.3 mm min^{-1} were used. The compression test was stopped after a 5 mm displacement was reached. For the tensile testing, a preload force of 50 N and a displacement rate of 5 mm min^{-1} were used. The strain in the test component was measured using an extensometer with 1 μm accuracy. For the flexural testing, a three-point-bending set up was used with a support span of 32 mm and support and nose diameter of 10 mm. For the test, a preload of 10 N and a displacement rate of 8.5 mm min^{-1} were used. Flexural tests were ended at a maximum displacement of 8 mm.

Samples dimensional accuracy was controlled using a micrometric digital caliper and weight accuracy using a Mettler Toledo Classic analytical balance (readability 0.1 mg).

Molecular Organic Contamination (MOC) was performed by mean of FTIR analysis using ZnSe windows for in-situ collection of contaminants. This measurement was performed following the ECSS-Q-ST-70-05C space standard [8]. Two MOC sampling were performed in vacuum condition: while printing and with the printer on but not printing. For both experiments, the ZnSe windows were placed at the same location. The two sampling condition used for MOC collection are presented in Table 1 hereafter.

Table 1 Conditions used for MOC collection in vacuum

MOC collection	Events time line (min)				
	$t = 0$	$t + 35$	$t + 45$	$t + 120$	$t + 160$
While printing in vacuum	Pump on Printer on	Pump off 10 mbar	Printing start 10 mbar	Print Stop 10 mbar	Printer cooled Venting
In vacuum	Pump on Printer on	Pump off 10 mbar	10 mbar	10 mbar	Venting

3 Results and discussion

To control the accuracy of the manufacturing process and the difference that might occur due to the vacuum environment, all produced samples are measured and weighted. The results are summarized in Table 2 where the average dimension and weight per sample type as a function of the environment (1 bar and 10 mbar) is compared against the dimension, volume, and weight as per design. The theoretical weight of a 100% dense part has been calculated using the theoretical volume of each design from the CAD file and the theoretical density of the polycarbonate material mentioned in the datasheet of the material supplier (1.19 g cm^{-3}). Volume measurement was discarded for the tensile test specimens due to their non-regular shape.

It is well established that the difference occurring between the initial design and the dimension after manufacturing is related to the intrinsic 3D printer capability and accuracy (positioning accuracy, nozzle diameter) and the proper adjustment of printing parameters like the printing speed, layer height, and raster angle for example. This relation between the printing parameters and the part dimensional accuracy has been subjected to many studies including optimized design of experiment [9, 10]. In the present work, printing parameters are fixed allowing a one-to-one comparison related to the effect of the processing environment only. The dimensional deviation occurring after printing compared to the initial design is also clear in the present work. However, these deviations are quite similar irrespectively of the environment used during printing.

It can be seen in Table 2 that the thickness of every flexural component produced is larger than the nominal height of 2 mm showing a deviation of 7–8% compare to the design value. This effect is due to the surface finishing capability and resulting roughness induced by the printing that was observed on the top of all flexural components. The same thickness deviation can be noticed for the tensile test specimens produced. These deviations obviously affect the calculation of volume and results in deviation of the calculated density. However, the density calculation expressed using this method is not optimal and shall be used only for a process evaluation and not for qualification purpose. Indeed, the measured volume of the part is considered to be 100% dense. However, FFF technology often results in void formation and therefore not 100% dense objects are produced. The presence of void has not been evaluated in this work and will definitely affect the effective density of the part.

The maximum strength of all mechanical test performed is plotted in Fig. 3. All tested samples exhibit reproducible results with low standard deviation whereas being printed at 1 bar or 10 mbar. It is clear that printing in vacuum condition does not have any strong negative effect on the mechanical properties at yield.

Compared to atmospheric condition, vacuum condition generates a decrease of 1.7% for flexural strength and an increase of 5.4% and 11.2% for tensile and compressive strength, respectively. Other noticeable effect of the vacuum environment on mechanical performance can be seen in Table 3.

Whereas the printing environment does not affect the tensile modulus, the ultimate tensile strength and

Table 2 Parts dimensional accuracy and deviation compared to initial design manufactures at 1 bar and 10 mbar (Volume and density are calculated using measured values of the geometry and theoretical value of the density—all average and Sd values presented in the table were rounded—deviations were calculated with non-rounded values)

Sample type	As per design	As manufactured @ 1 bar			As manufactured @ 10 mbar		
		Average	Sd	Deviation (%)	Average	Sd	Deviation (%)
Tensile							
Width (mm)	13.00	*13.14*	*0.05*	*1.07*	13.22	0.02	1.70
Thickness (mm)	3.20	*3.34*	*0.03*	*4.51*	3.28	0.03	2.67
Weight (g)	12.46	*12.37*	*0.03*	*− 0.67*	12.33	0.07	− 1.02
Compression							
Diameter (mm)	12.70	12.78	0.03	0.61	12.735	0.05	0.28
Height (mm)	25.40	25.35	0.29	− 0.18	25.251	0.02	− 0.59
Weight (g)	3.83	3.79	0.03	− 0.86	3.758	0.03	− 1.85
Volume (mm^3)	3217	3251	20.09	1.04	3216	24.24	− 0.03
Density (g cm^{-3})	1.19	*1.167*	–	*− 1.88*	*1.168*	–	*− 1.82*
Flexural							
Width (mm)	12.70	12.69	0.03	− 0.05	12.78	0.01	0.67
Thickness (mm)	2.00	2.16	0.01	7.96	2.14	0.03	7.28
Length (mm)	50.00	49.95	0.02	− 0.10	50.00	0.30	0.02
Weight (g)	1.51	1.53	0.01	1.06	1.50	0.01	− 0.31
Volume (mm^3)	1270	1369	11.14	7.80	1372	15.89	8.01
Density (g cm^{-3})	1.19	*1.11*	–	*− 6.27*	*1.10*	–	*− 7.73*
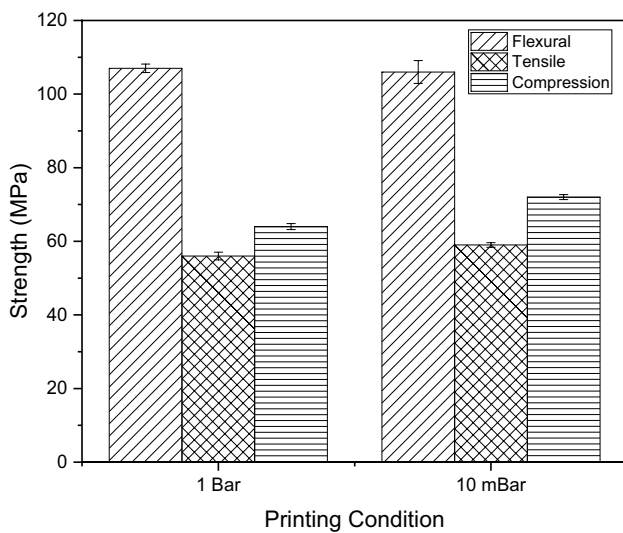
Fig. 3 Average flexural, tensile, and compressive maximum strength of tested specimens as a function of the printing environment pressure

associated strain differs significantly. On one hand, the vacuum condition reduces the strength at break by 9.3% and on the other hand, the strain at break increase by 64% due to vacuum condition. The failure type is presented in Fig. 4. The sample printed at 1 bar always presents a clear fracture perpendicular to the tensile load whereas the samples printed at 10 mbar always present a fracture with a 45° orientation. Necking and strong plastic deformation including tendrils is very well pronounced on samples printed in vacuum. The parts printed at 10 mbar clearly exhibit a more ductile behavior compared to the one printed at 1 bar that are comparatively more brittle.
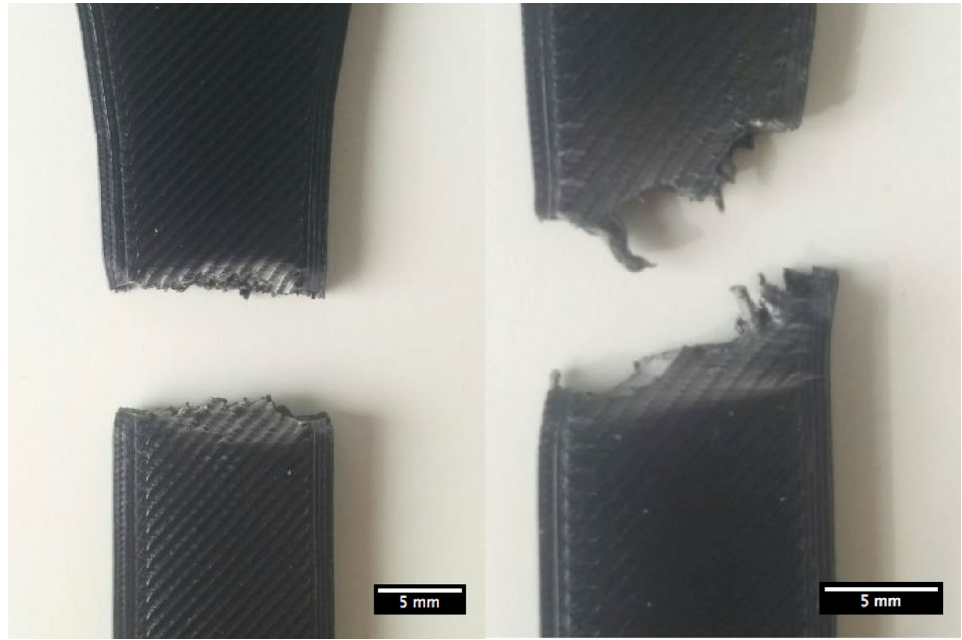
Similar improvements due to vacuum are also occurring during compressive load. Samples printed in vacuum exhibit a significant increase of compressive strength and are subjected to 13% less deformation (Fig. 5). The flexural tests present quite similar results with a deviation below 2% between the two processing condition (Fig. 5). The overall improvement in mechanical performance in the vacuum can be related to several aspect. The poor thermal transfer in a vacuum could generate better welding between polymer threads. Indeed, a better temperature homogeneity at part level and a slower cooling will be favorable for intermolecular chain diffusion between each printed layer. Another hypothesis is related to the fact that in vacuum, there will be a lower amount of defect/voids and at the same time a homogenization of their shape (rounder), size and distribution. This last hypothesis needs to be investigated further as defect type, size and distribution within the part will have an effect on the mechanical performance. Having a process that generates defects that are more homogeneous, reproducible and controllable may ease the manufacturing process qualification and have a positive outcome on part acceptance and quality.

Looking into space application and implementation of such process out-of-earth, cleanliness and contamination aspect are of paramount importance. The results of the MOC analysis performed show that the printing process in vacuum result in a marginal increase of MOC (Table 4). Outgassing compliance for material for space application are based on a specific test performed in high vacuum and at 125 °C; well described in NASA and Space European standard [11]. Even if some PC blends can be outgassing compliant according to European and NASA standard, having it processed at 260 °C in its melt state at 10 mbar it was feared to generate an increase of molecular contamination. Only hydrocarbon

Sample type	@ 1 bar		@ 10 mbar		Change due to vacuum (%)
	Average	Sd	Average	Sd	
Tensile					
Modulus (GPa)	1.9	0.04	1.9	0.05	+0.5
Ultimate tensile strength (MPa)	56.2	1.02	59.3	0.62	+5.4
Strain (%)	4.4	0.19	4.6	0.13	+4.5
Strength at break (MPa)	51.9	1.32	47.1	1.41	−9.3
Strain at break (%)	7.0	0.52	11.5	1.14	+64
Compression					
Modulus (GPa)	1.6	0.03	1.7	0.02	+7.5
Maximum strength (MPa)	64.5	0.67	71.7	0.80	+11.2
Strain (%)	−14.8	0.80	−12.9	0.14	−13
Flexural					
Modulus (GPa)	2.4	0.04	2.3	0.05	−2.6
Maximum strength (MPa)	107.7	1.14	105.9	3.11	−1.7
Strain (%)	6.27	0.38	6.30	0.43	+0.4

Table 3 Comparison of mechanical test results average ($n = 5$) with standard deviation (Sd) for sample produced at 1 bar and 10 mbar

Fig. 4 Fracture zone for tensile test specimen printed at 1 bar (left) and 10 mbar (right)

Fig. 5 Sample after compression manufactured at 1 bar (**a**) and at 10 mbar (**b**). Flexural test sample manufactured at 1 bar (**c**) and 10 mbar (**d**)
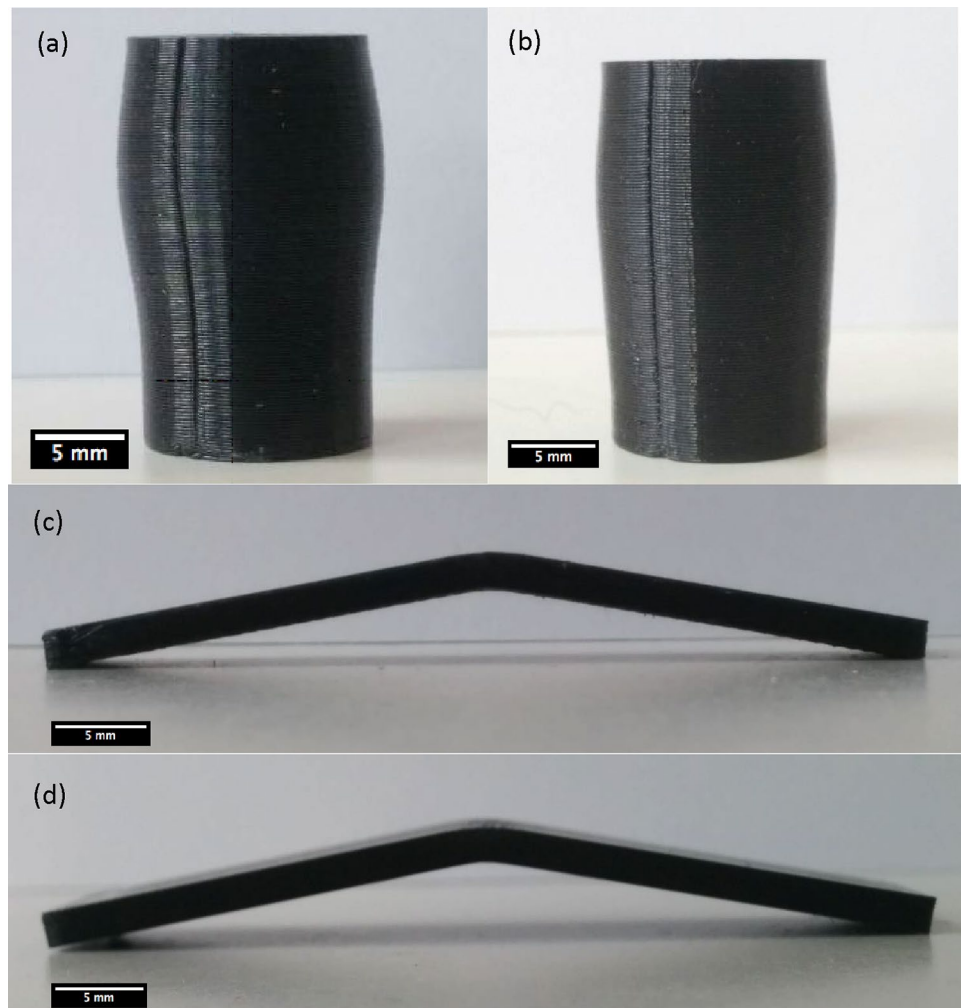
Table 4 Molecular organic contamination value given in 10^{-7} g cm^{-2}

MOC collection	Hydrocarbon	Ester	Methyl silicones	Methyl-phenyl silicones	Total MOC
While printing in vacuum	0.6	< 0.5	< 0.1	< 0.2	0.6
In vacuum	0.5	< 0.5	< 0.1	< 0.2	0.5

could be detected with a difference of 1.10^{-8} g cm^{-2} between the printer being in steady-state in vacuum and the printer printing for an effective period of 125 min (time between the vacuum chamber reach 10 mbar and is isolated until venting). The final amount of the molecular contaminants collected ($6 \cdot 10^{-8}$ g cm^{-2}) mainly origin form the printer and its components. This molecular contamination is not seen as a huge risk knowing that the hardware has not been designed for space application and could be mitigated by implementing space compliant materials for the hardware design and a contamination mitigation philosophy based on space standard (i.e. bake out).

From the results presented, the FFF process operated under 10 mbar pressure and 1 g of gravity is able to produce parts with similar or better properties compared to a ground environment in atmospheric pressure. It is already demonstrated that FFF process can be operated under a microgravity environment with normal conditions of temperature and pressure [2, 5]. The 3D printing in zero g technology demonstration mission from NASA on board the ISS were performed using a 3D printer designed to meet ISS operational condition in a closed and controlled environment and ABS material [4]. Using high-performance thermoplastic like polyetheretherketone, the FFF process was capable to produce parts operated in an inverted gravity vector (in -1 g condition) with equivalent mechanical performance as per normal condition (in 1 g) [12]. In this respect, with the results from this study, the operation of a 3D printer in low vacuum condition and microgravity environment should not raise any concern with a wide range of thermoplastics. However, looking at an implementation in space, it is necessary to assess the capability of the FFF process to operate in high vacuum (10^{-5}–10^{-7} mbar) more representative of the space environment. In the long term, this will need to be done considering thermal aspect leading to new design consideration to enable the FFF process to be operated in space.

4 Conclusion

The results presented in this work are quite encouraging demonstrating that FFF process, even based on commercially available off-the-shelf, is suitable for low vacuum environment to produce parts with the same accuracy as in normal condition. In addition, it has been shown that the mechanical performance of the parts printed in vacuum exhibit better performance in tension and compression and present a more ductile behavior. From a cleanliness and contamination aspect, it is shown that the process can be fit for purpose and that the hardware can have a strong contribution to the molecular contamination during the operational phase. These results and proof of concept indicate that a printer based on FFF process fully optimized for a space vacuum environment using space-compliant thermoplastics (i.e. PEEK, PEI) could be implemented to manufacture large, high-performance parts in space, in-orbit or on planet in the future.

References

1. Moraguez, M., De Weck, O.: Benefits of in-space manufacturing technology development for human spaceflight. In: 2020 IEEE Aerospace Conference, pp. 1–11. (2020)
2. Prater, T., Bean, Q., Werkheiser, N., Grguel, R., Beshears, R., Rolin, T., Huff, T., Ryan, R., Ledbetter, F., Ordonez, E.: Analysis of specimens from phase I of the 3D printing in Zero G technology demonstration mission. Rapid Prototyp. J. **23**, 1212–1225 (2017). https://doi.org/10.1108/RPJ-09-2016-0142
3. Werkheiser, M.J., Dunn, J., Snyder, M.P., Edmunson, J., Cooper, K., Johnston, M.M.: 3D printing in Zero-G ISS technology demonstration. In: AIAA SPACE 2014 Conference and Exposition, p. 4470. (2014)
4. Prater, T., Werkheiser, N., Ledbetter, F., Timucin, D., Wheeler, K., Snyder, M.: 3D Printing in Zero G Technology Demonstration Mission: complete experimental results and summary of related material modeling efforts. Int. J. Adv. Manuf. Technol. **101**, 391–417 (2019). https://doi.org/10.1007/s00170-018-2827-7
5. Musso, G., Lentini, G., Enrietti, L., Volpe, C., Ambrosio, E.P., Lorusso, M., Mascetti, G., Valentini, G.: Portable on orbit printer 3D: 1st European additive manufacturing machine on international space station. In: Advances in Physical Ergonomics and Human Factors, pp. 643–655. Springer, Cham (2016)
6. Prater, T., Werkheiser, N., Ledbetter, F., Morgan, K.: In-space manufacturing at NASA marshall space flight center: a portfolio of fabrication and recycling technology development for the international space station. In: 2018 AIAA SPACE and Astronautics Forum and Exposition, p. 5364. (2018)
7. Quinn, M., Guo, J., Lafont, U., Versteegh, J.: Fused filament fabrication of polycarbonate components in a simulated on-orbit environment. In: Proceedings of the 69th International Astronautical

Congress (IAC 2018). International Astronautical Federation, IAF (2018)

8. European Cooperation for Space Standardization: ECSS-Q-ST-70–05C Rev.1: Detection of organic contamination surfaces by IR spectroscopy. (2019)

9. Kohad, A., Dalu, R.: Optimization of process parameters in fused deposition modeling: a review. Int. J. Innov. Res. Sci. Eng. Technol. **6**, 505-511 (2017)

10. Tiwari, K., Kumar, S.: Analysis of the factors affecting the dimensional accuracy of 3D printed products. Mater. Today: Proc. **5**, 18674–18680 (2018)

11. European Cooperation For Space Standardization: ECSS-Q-ST-70-02C: Thermal vacuum outgassing test for the screening of space materials. (2008)

12. Daurskikh, A., Sgambati, A., Graça, D., Berg, M., Baptista, A., Angelo, M., Lafont, U.: Influence of spatial orientation on properties of 3D printed PEEK parts and their design adaptation. In: Proceedings of the 69th International Astronautical Congress (IAC 2018). International Astronautical Federation, IAF (2018)